Interaction of the G′ Domain of Elongation Factor G and the C-Terminal Domain of Ribosomal Protein L7/L12 during Translocation as Revealed by Cryo-EM

ARTICLE *in* MOLECULAR CELL · JANUARY 2006

Impact Factor: 14.02 · DOI: 10.1016/j.molcel.2005.10.028 · Source: PubMed

5 AUTHORS, INCLUDING:

Manjuli R Sharma
Wadsworth Center, NYS Department of He…
27 PUBLICATIONS **1,214** CITATIONS

SEE PROFILE

Rajendra K Agrawal
Wadsworth Center, NYS Department of He…
74 PUBLICATIONS **3,046** CITATIONS

SEE PROFILE

Molecular Cell, Vol. 20, 723–731, December 9, 2005, Copyright ©2005 by Elsevier Inc. DOI 10.1016/j.molcel.2005.10.028

Interaction of the G′ Domain of Elongation Factor G and the C-Terminal Domain of Ribosomal Protein L7/L12 during Translocation as Revealed by Cryo-EM

Partha P. Datta,[1] Manjuli R. Sharma,[1] Li Qi,[1,2] Joachim Frank,[1,2] and Rajendra K. Agrawal[1,2,*]
[1] Division of Molecular Medicine
Wadsworth Center
New York State Department of Health
Empire State Plaza
P.O. Box 509
Albany, New York 12201
[2] Department of Biomedical Sciences
The State University of New York at Albany
Albany, New York 12201

Summary

During tRNA translocation on the ribosome, an arc-like connection (ALC) is formed between the G′ domain of elongation factor G (EF-G) and the L7/L12-stalk base of the large ribosomal subunit in the GDP state. To delineate the boundary of EF-G within the ALC, we tagged an amino acid residue near the tip of the G′ domain of EF-G with undecagold, which was then visualized with three-dimensional cryo-electron microscopy (cryo-EM). Two distinct positions for the undecagold, observed in the GTP-state and GDP-state cryo-EM maps of the ribosome bound EF-G, allowed us to determine the movement of the labeled amino acid. Molecular analyses of the cryo-EM maps show: (1) that three structural components, the N-terminal domain of ribosomal protein L11, the C-terminal domain of ribosomal protein L7/L12, and the G′ domain of EF-G, participate in formation of the ALC; and (2) that both EF-G and the ribosomal protein L7/L12 undergo large conformational changes to form the ALC.

Introduction

Ribosomes provide the platform for polypeptide synthesis in all organisms. The *Escherichia coli* 70S ribosome is composed of two subunits of unequal sizes. The small 30S subunit contains 21 proteins (numbered S1–S21) and a 16S RNA molecule, whereas the large 50S subunit contains 33 proteins (numbered L1–L34) and two rRNA molecules (5S and 23S) (Wittmann-Liebold, 1985). Among the large-subunit proteins, L7 and L12 are identical, except that the N terminus of L7 is posttranslationally acetylated (see Traut et al., 1995). After peptide-bond formation on the ribosome, the A and P site tRNAs move to the P and E sites, respectively, with the concomitant procession of the mRNA by one codon. This process is called translocation and is catalyzed by elongation factor G (EF-G) in the presence of GTP. After GTP is hydrolyzed to GDP, inorganic phosphate (P_i) is released (Ishitsuka et al., 1970; Rodnina et al., 1997) and EF-G dissociates from the ribosome.

Previous biochemical studies (Dey et al., 1995; Savelsbergh et al., 2000) have shown that in vitro interaction of L7/L12 (the only ribosomal protein that is present in four copies in most organisms [see Traut et al., 1995] or in six copies in thermophiles [see Diaconu et al., 2005]; it constitutes a stalk-like feature of the large subunit of the ribosome) with EF-G leads to an increased GTPase activity of EF-G. On the ribosome, hydrolysis of GTP by EF-G and EF-Tu (another elongation factor that delivers aminoacyl-tRNA to the ribosome) is accelerated by at least seven orders of magnitude (Parmeggiani and Sander, 1981; Pape et al., 1998; Rodnina et al., 1996, 1997). If the L7/L12 stalk is removed from the ribosome, the GTPase activity drastically decreases by 4000-fold (Mohr et al., 2002). These studies have implicated a direct involvement of L7/L12 in the EF-G-dependent reactions. Interaction of EF-G with the ribosome in two functional states, namely the GTP and GDP states, has been studied earlier by three-dimensional (3D) cryo-EM (Agrawal et al., 1998, 1999; Stark et al., 2000; Valle et al., 2003). These studies revealed extensive conformational changes in both EF-G and the ribosome. It was found that the EF-G-dependent reaction is accompanied by a ratchet-like rotation of the two ribosomal subunits (Agrawal et al., 1999; Frank and Agrawal, 2000, 2001).

Among several conformational changes, the formation of an ALC between the stalk-base region of the ribosome and the G′ domain of EF-G, in the GDP state, has been observed (Agrawal et al., 1998, 1999). These studies also showed that formation of the ALC is independent of the presence of tRNA(s) on the ribosome. The ALC was tentatively interpreted to represent the C-terminal domain of L7/L12 (L7/L12-CTD) (Agrawal et al., 1998). To understand the molecular interactions between EF-G and the ribosome, we fitted the X-ray crystallographic structure of EF-G into the corresponding cryo-EM density mass in both the GTP- and GDP-state maps. Even though most of the EF-G domains fit quite well in the GDP-state map, the composition of the ALC could not be explained unequivocally from our previous ~18 Å resolution cryo-EM map. However, the N-terminal domain of ribosomal protein L11 (L11-NTD) was implicated in the formation of the ALC, at the end of the structure that is contiguous with the ribosome (Agrawal et al., 2001). Further studies, involving a flexible-docking approach (Wriggers et al., 2000) and higher-resolution cryo-EM maps (Gao et al., 2003; Valle et al., 2003), have failed to elucidate the nature of the ALC, leaving open the question of whether the ALC is an extension of EF-G, a protrusion of the ribosome itself, or a structure shared between the two.

In order to delineate the connecting mass within the ALC, we selected a single amino acid, Ala 209, within the G′ domain of the *E. coli* EF-G sequence (Ovchinnikov Yu et al., 1982; Zengel et al., 1984) as the target site for labeling with monomaleimido undecagold, a heavy-metal-cluster compound (Safer et al., 1986; Hainfeld, 1987), and for subsequent visualization of this electron-dense label by single-particle 3D cryo-EM (Frank et al., 2000). Our study demonstrated that a single undecagold (UG; an 11 gold-atom cluster) can be visualized within the ribosome. Furthermore, the movement of the

*Correspondence: agrawal@wadsworth.org

UG-labeled amino acid during translocation could be inferred by locating the UG in two functional states. By taking into consideration the UG position within the cryo-EM envelope, we were able to fit the atomic structures of EF-G and adjacent ribosomal components into the cryo-EM maps. Our study has delineated the boundary of EF-G within the ALC and has also shown that the L7/L12-CTD is directly involved in the formation of the ALC.

Results and Discussion

Labeling of EF-G with Electron-Dense Gold Clusters and Localization of the Label in Two Functional States of the Ribosome

We have targeted an amino acid residue at position 209 of *E. coli* EF-G (Ovchinnikov Yu et al., 1982; Zengel et al., 1984). Position 209 is located near the tip of the G′ domain of EF-G (AEvarsson et al., 1994; Czworkowski et al., 1994), which, according to earlier cryo-EM results, appears to make a direct contact with the stalk-base region of the ribosome (Agrawal et al., 1999). We used monomaleimido-UG (core diameter ~8 Å, Nanoprobes Inc., Yaphank, NY), which forms a covalent linkage with the SH group of the cysteine (Cys) residue (Safer et al., 1986; Hainfeld, 1987) and can be visualized by 3D cryo-EM (Kikkawa et al., 2000; Al-Bassam et al., 2002). There are three naturally occurring Cys residues in *E. coli* EF-G (Ovchinnikov Yu et al., 1982; Zengel et al., 1984). Because these Cys residues are not located at strategic 3D positions, we replaced them with other amino acids by point mutations (see Experimental Procedures) such that the biological activity of EF-G is not affected (also see Wilson and Noller, 1998). Finally, we introduced a Cys residue at our target location 209, which is naturally an alanine. Henceforth, we will refer to the mutated EF-G with a Cys at 209 as "EF-G-209C." The EF-G-209C was then labeled with monomaleimido-UG (EF-G-209C-UG) and purified through several rounds of HPLC. The extent of UG labeling in the HPLC fractions pooled as EF-G-209C-UG was ~95%, as ascertained spectrophotometrically (see the Supplemental Data available with this article online). It should be noted that the purification of the UG-labeled EF-G from unlabeled EF-G was a necessary and critical step for the localization of the UG signal on the ribosome bound EF-G.

EF-G-209C-UG binds to the ribosome in both the GTP (70S•EF-G-209C-UG•GMPPCP complex) and the GDP (70S•EF-G-209C-UG•GDP•fusidic acid complex) states with high occupancy (Figure 1A). The extent of binding was close to that observed for the binding of unlabeled-EF-G-209C in both 70S•EF-G-209C•GMPPCP and 70S•EF-G-209C•GDP•fusidic acid complexes. Three-dimensional cryo-EM maps of all four complexes (two containing EF-G-209C-UG in GTP and GDP states and their respective controls) were obtained in the 11.2–12.2 Å resolution range, according to the Fourier shell correlation (FSC) criterion with a 0.5 cutoff (Bottcher et al., 1997; Malhotra et al., 1998), or in the 7.8–9.0 Å range, according to the 3σ criterion (Orlova et al., 1997) (see Figure S2 and Table S1).

Comparison of the maps of UG-labeled complexes with respective controls reveals that the overall shape of the labeled region (i.e., the ALC region) does not change with the incorporation of the UG label, except that an additional mass is seen near the tip of the G′ domain of EF-G in both GTP and GDP states (Figures 1B and 1C). In the GDP state, this density is closer to the ribosomal 50S subunit. The additional mass can be readily attributed to the electron-dense UG. We calculated

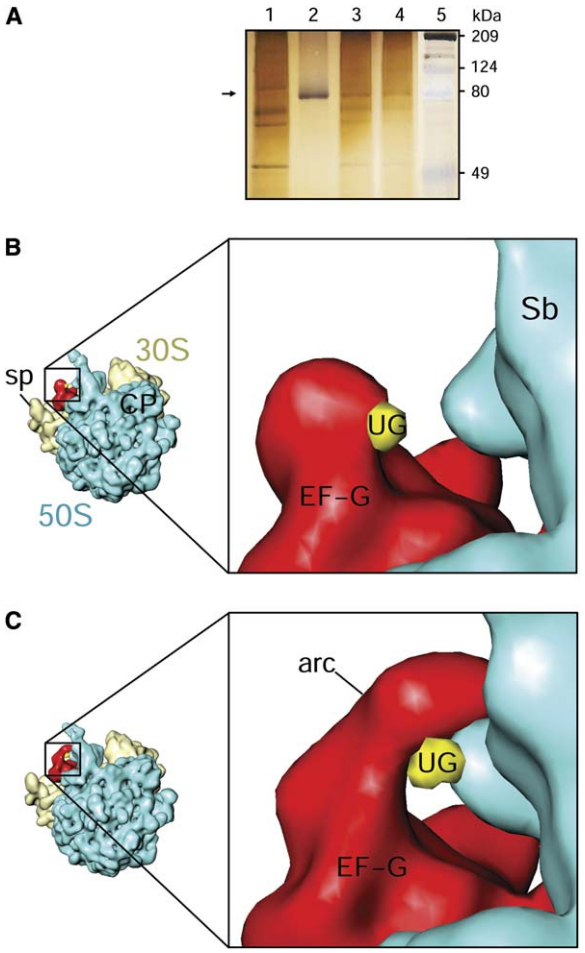

Figure 1. Binding of UG-Labeled EF-G-209C to the *E. coli* 70S Ribosome and Visualization of UG in the 3D Cryo-EM Maps of the Ribosome•EF-G Complexes in the GTP and GDP States

(A) Lanes 3 and 4 of the silver-stained SDS-PAGE gel show the binding of EF-G-209C-UG to the 70S ribosome in the GTP state (in the presence of GMPPCP) and in the GDP state (in the presence of GTP and fusidic aid), respectively. Lanes 1, 2, and 5 show control 70S ribosome, HPLC-purified EFG-209C-UG (position marked by an arrow on the left), and a molecular-mass ladder, respectively. Only the relevant upper portion of the gel is shown.

(B and C) Difference maps (golden yellow), computed between the 3D cryo-EM maps of the 70S ribosome•EF-G-209C complexes with and without UG, are superimposed on the map of the 70S•EF-G-209C•GMPPCP complex (B) and on the 70S•EF-G-209C•GDP•fusidic acid complex (C), respectively. (C) shows the ALC (arc) formation between EF-G (red) and the L7/L12 stalk base of the 50S ribosomal subunit. The UG density (golden yellow) has moved toward the stalk base, as compared to its location in (B). The ribosome is shown from its 50S-subunit side (see thumbnail images, left-hand margin), so as to reveal the positions of the UG density. Landmarks of the 50S subunit (blue) are: CP, central protuberance; and Sb, protein L7/L12 stalk base. The landmark of the 30S subunit (yellow, in the thumbnail images) is: sp, spur. For a direct comparison between the maps of UG-labeled and unlabeled 70S•EF-G-209C complexes in both GTP and GDP states see Figure S3.

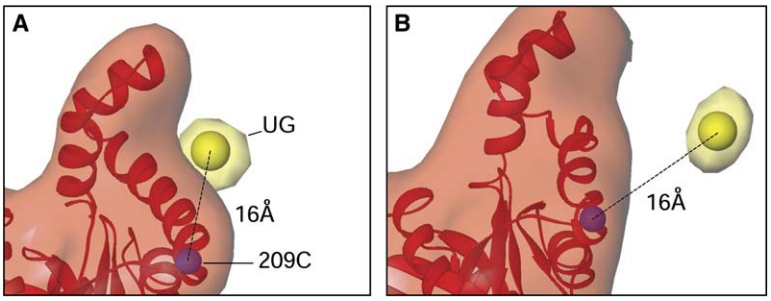

Figure 2. Localization of Amino Acid 209C in EF-G

The X-ray crystallographic structure of EF-G was docked into the corresponding cryo-EM densities of EF-G within the (A) EF-G-209C-UG•GMPPCP and (B) EF-G-209C-UG•GDP•fusidic acid complex maps, taking into consideration the constraints imposed by both the cryo-EM envelope (semitransparent red) and the positions of UG (semitransparent yellow). The cryo-EM maps are displayed at threshold values that are slightly higher than those used in Figure 1. The locations of the C_α atom of residue 209C (blue) within the G domains of EF-G (red) and of the core of the UG cluster (golden yellow) are marked by spheres. Based on the positions of 209C determined in the GTP and GDP states, the residue moves by ~7 Å. It should be noted that the directions of movement of 209C and UG are in slightly different planes.

difference maps for the GTP state by subtracting the 3D map of the 70S•EF-G-209C•GMPPCP complex from that of the 70S•EF-G-209C-UG•GMPPCP complex, and likewise for the GDP state by subtracting the 3D map of the 70S•EF-G-209C•GDP•fusidic acid complex from that of the 70S•EF-G-209C-UG•GDP•fusidic acid complex. In both cases, the difference maps contained a sharply defined density peak (represented by golden-yellow subspherical masses in Figures 1B and 1C). In order to further validate the localization of UG, we also computed the difference maps between additional maps (UG-labeled and unlabeled) that had been calculated exclusively from the data set collected at close-to-focus settings of the electron microscope. As reported earlier (Wagenknecht et al., 1994), UG densities so obtained are more sharply defined and their locations are highly reproducible.

The two positions of the density, corresponding to UG in the two functional states, revealed a marked shift: they differed by ~17Å, indicating that the target amino acid (209C) of the G′ domain of EF-G has moved by this amount. However, in order to accommodate a movement of such a large magnitude, the G and G′ domains of EF-G must have undergone a large conformational rearrangement. A rearrangement is indeed readily evident from a visual comparison of the EF-G densities in the GTP and GDP states (compare [B] and [C] in Figure 1): the G′ domain of EF-G in the latter state significantly elongates and extends toward the L7/L12-stalk base of the 50S ribosomal subunit. It should be noted that we initially used monomaleimido-Nanogold (NG; a larger gold cluster with a core diameter of ~14 Å) for the labeling of the same amino acid (209C). However, EF-G-209C-NG was found to bind to the 70S ribosome in the GTP state, but not in the GDP state, suggesting that (1) the formation of the ALC was prevented, presumably due to steric hindrance caused by the larger size of NG, and (2) the formation of the ALC is important for the transient binding of EF-G to the ribosome after GTP hydrolysis.

Docking of the Atomic Structure of EF-G into the Cryo-EM Maps

To localize the target amino acid 209C in EF-G in the two functional states, we fitted an atomic model of EF-G (AEvarsson et al., 1994) into the corresponding mass in the cryo-EM maps, taking into consideration both the cryo-EM envelope and the positional constraints imposed by the UG density. For an optimum fit, we had to separately dock the G and G′ domains, which together constitute domain I of EF-G (AEvarsson et al., 1994; Czworkowski et al., 1994), as two rigid bodies into our cryo-EM maps. Further changes within these subdomains were also necessary to satisfy both the cryo-EM envelope and the position of the UG. A combination of manual rigid-body docking and flexible docking (Wriggers et al., 2000) approaches was used for the fitting of the G′ domain; the unstructured linker regions within the G′ domain were allowed to stretch, whereas the secondary structure (α helices) was kept intact. During this process, stereochemical constraints were taken into consideration, and the fitted structures were subjected to energy minimization. We assessed the quality of fits by calculating cross-correlation coefficients (Agrawal et al., 1998, 2004; Sharma et al., 2005). In our final fittings, position 209 of EF-G is situated ~16 Å away from the UG label (Figures 2A and 2B), as would be expected when the length of the linker and the radius of the organic shell that surrounds the UG core are taken into account (Safer, 1999). Based on these fittings, we find that the target amino acid residue has moved by ~7 Å in the GDP state from its position in the GTP state (Figure 2C), suggesting that a portion of the spatial shift observed in the UG density is due to local conformational change of the G′ domain of EF-G.

Composition of the ALC

To interpret the remaining portion of the ALC, we fitted X-ray crystallographic structures of protein L11 and the 58 nucleotide L11-associated 23S rRNA segment (Wimberly et al., 1999) into the stalk-base region of our cryo-EM maps. In contrast to a previous low-resolution study (Agrawal et al., 2001), these fittings were guided by the presence of strong structural features for both the 58-nucleotide L11-associated 23S rRNA segment and protein L11 in the density maps; these features restricted any major reorientation of L11-NTD between GTP and GDP states. Therefore, the fittings resulted in a significant gap (~21 Å) between the closest atoms of L11-NTD and the tip of the G′ domain of EF-G, leaving unexplained a large mass within the ALC (Figure 3A). However, this unexplained density overlaps with an as-yet uncharacterized mass that protrudes from the stalk-base region in the 3D maps of both empty control

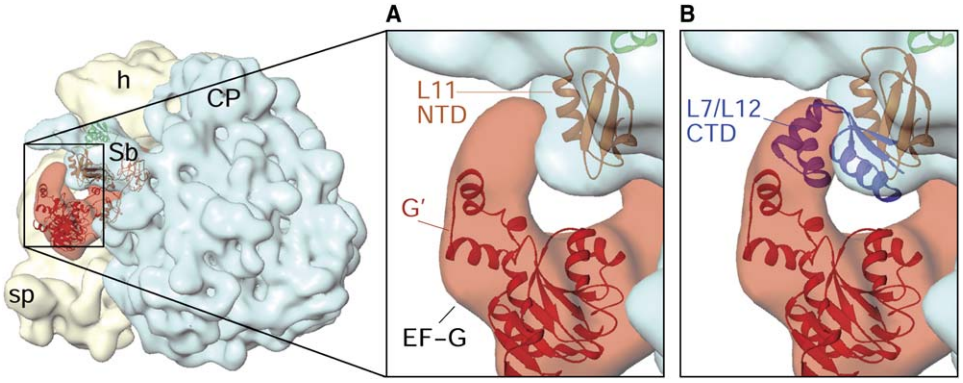

Figure 3. Participation of EF-G in ALC Formation

(A) Relevant portions of EF-G (semi-transparent red) and the stalk base of the 50S subunit (semitransparent blue) are shown enlarged, with atomic structures (ribbons) of EF-G (G and G′ domain, red) and the L11-NTD (orange) fitted into the corresponding cryo-EM densities. An ~21 Å gap between the tips of EF-G and the L11-NTD is observed.

(B) Fitting of the atomic structure of the L7/L12-CTD (blue ribbons) into remaining density within the ALC that could not be attributed to either L11 or any of EF-G's domains. Densities (representing portions of both the ribosome and EF-G) present in planes behind the features of interest have been computationally removed in both panels for visual clarity. It should be noted that atomic structures of all components of the ribosome and EF-G were fitted into the cryo-EM map; however, only relevant fittings are shown in this and subsequent figures. The orientation of the 70S•EF-G-209C-UG•GDP•fusidic acid complex is shown to the left of (A). Landmarks include: h, 30S subunit head. All other landmarks are either self-explanatory or have been introduced in Figure 1.

and GTP-state ribosomes (region identified by an asterisk in Figure 4A). In the GDP state, this protrusion contributes to the formation of the ALC. Because this protruded structure cannot be explained either by any of the EF-G domains or by the L11-NTD, and because it is observed in both UG-labeled and unlabeled EF-G-ribosome complexes, it most likely represents the CTD of one of the four copies of the L7/L12 protein (see below) of the 50S ribosomal subunit. It should be noted that a similar ALC was also observed in the ribosome complex with EF-Tu (Stark et al., 1997) and, more recently, the complex with initiation factor 2 (Allen et al., 2005), where it was tentatively interpreted to represent L7/L12-CTD.

The L7/L12-CTD has been strongly implicated in EF-G binding, as truncated L7/L12 fragments lacking the CTD fail to support protein synthesis even though they bind to the ribosome (van Agthoven et al., 1975; Kotelianskyet al., 1978). Furthermore, antibodies to the CTD inhibit the binding of elongation factors and protein synthesis in general (Sommer et al., 1985). The L7/L12-CTD is highly mobile and has been suggested to move as far as 50 Å away from the L7/L12-NTD (Traut et al., 1995). However, its primary attachment through the NTD to the large ribosomal subunit is ~44 Å away (Diaconu et al., 2005) from the ALC seen in our map. Therefore, it is conceivable that one of the four L7/L12-CTD copies is directly involved in the formation of the ALC. The stalk region is composed of proteins L11, L10, L7/L12 (Traut et al., 1995; Diaconu et al., 2005), and the L11-associated 23S rRNA segment (Wimberly et al., 1999). It has been shown that the L7/L12-CTD crosslinks strongly to proteins L11 (Dey et al., 1998) and L10 (Makarov et al., 1993). The L7/L12-CTD has been localized in various other regions of the ribosome by crosslinking (see Traut et al., 1995) and, in the four most probable positions, by NG labeling and cryo-EM (Montesano-Roditis et al., 2001) in an ~30 Å resolution map of a reconstituted empty 70S ribosome. That study placed one of the four NG-derived positions of the L7/L12-CTD such that it would overlap with the ALC seen in our maps. Possible occupancy of the L7/L12-CTD near the factor binding domain of the 50S subunit was also suggested earlier by crosslinking experiments (Zecherle et al., 1992).

Because the features of unexplained density within the ALC (Figure 3A) match closely with the L7/L12-CTD, we docked the X-ray crystallographic structure of the L7/L12-CTD (Leijonmarck and Liljas, 1987) into the remaining ALC density (Figure 3B). The CTD structure fits tightly into the ALC, and the fit satisfies all previous biochemical observations. Even though the EF-G interaction with L7/L12 is known to increase the factor's GTPase activity, the site of interaction is not expected to be at the GTP catalysis center of EF-G (Mohr et al., 2002). Indeed, the fitted L7/L12-CTD in our map is ~30 Å away from the GTPase center of EF-G. In contrast to the previous low-resolution results (Agrawal et al., 2001), we find that the ALC is not contiguous with the tip of the L11-NTD within the stalk base, but instead extends from the globular core of the L11-NTD, such that the ALC is shifted more toward the ribosomal subunit: subunit interface side.

Dynamics of the L7/L12-CTD during EF-G-Dependent Translocation

We have analyzed the position and conformation of one of the four L7/L12-CTD copies in the maps of the 70S ribosome, in both the presence and absence of EF-G (Figures 4 and 5). We find that the L7/L12-CTD undergoes considerable conformational changes in association with the L11-NTD during the course of EF-G-dependent reactions (Figure 5). Density corresponding to the L7/L12-CTD becomes more defined upon EF-G binding and shifts toward the G′ domain of EF-G (Figure 4A, and compare [A] and [B] in Figure 5). Furthermore, the L7/L12-CTD twists slightly toward the G′ domain of EF-G upon GTP hydrolysis (Figure 4B, and compare [B]

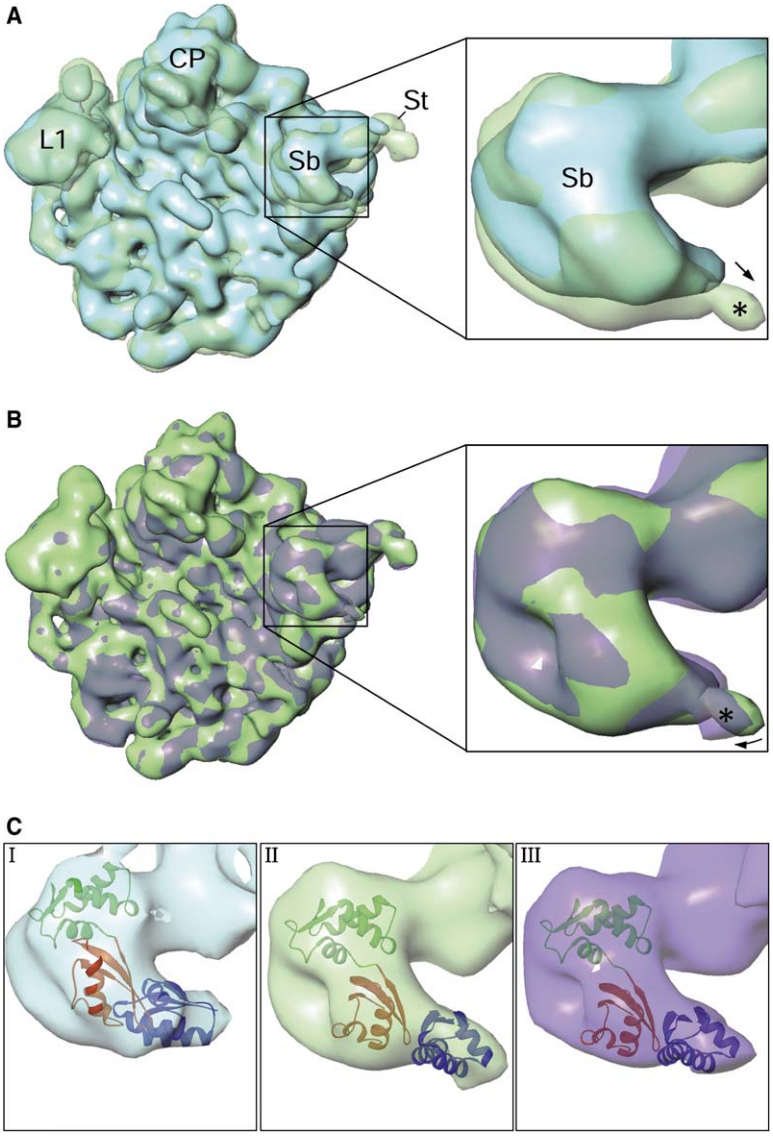

Figure 4. Conformational Change in the Stalk-Base Region of the Large Ribosomal Subunit upon EF-G Binding to the Ribosome and upon GTP Hydrolysis

(A) The large (50S) ribosomal subunit structures from the cryo-EM maps of the empty control 70S ribosome (solid blue) and the 70S•EF-G-209C•GMPPCP complex (semitransparent green) are superimposed. The stalk-base region is boxed and enlarged in the right-hand panel. While the whole stalk-base region shifts toward the small ribosomal subunit (also see Agrawal et al., 2001) upon EF-G binding, a marked shift (indicated by an arrow) in the putative L7/L12-CTD (a protruding density, marked by an asterisk) is observed.

(B) As in (A), a comparison of the stalk-base region from the maps of the 70S•EF-G-209C•GMPPCP (solid green) and the 70S•EF-G-209C•GDP•fusidic acid (semitransparent magenta) complexes is presented. The 50S map from the 70S•EF-G-209C•GDP•fusidic acid complex now includes the density assigned to L7/L12-CTD (see Figure 3B).

(C) The stalk-base regions in the control (I), the 70S•EF-G-209C•GMPPCP complex (II), and the 70S•EF-G-209C•GDP•fusidic acid complex (III) are shown, with atomic structures of L11 (NTD, orange; CTD, green ribbons) and L7/L12-CTD (blue ribbons) fitted into corresponding cryo-EM densities. The cryo-EM density of the control ribosome in (C[I]) is shown at a lower threshold value. Landmarks are as follows: St, L7/L12 stalk; L1, protein L1 protuberance. All other landmarks are as in previous figures.

and [C] in Figure 5). This twisting movement shifts the L7/L12-CTD's position from the interribosomal subunit side more toward the solvent side. Thus, we find that the L7/L12-CTD is indeed highly mobile during the course of the EF-G ribosome interaction. Based on our fittings of the L7/L12-CTD within the ALC and on the fitting of the L7/L12-NTD within the extended stalk in a recent structural study (Diaconu et al., 2005), we are now able to locate positions of both the CTD and NTD of one of the four copies of L7/L12 on the large subunit of the EF-G bound ribosome (Figure 6). A further analysis of our dockings suggests that, at any given time (i.e., with a defined orientation of L10 bound L7/L12-NTDs on the ribosome; see Diaconu et al., 2005), only two of the four copies of L7/L12-CTD has the potential to reach the site of ALC formation. The remaining two copies of the CTD, in fact, would be directed away from the ALC.

Dynamic interactions between the L7/L12-CTD and the G′ domain of EF-G apparently follow a cyclic process by which, upon GTP hydrolysis, a part of EF-G (domain V) pushes the L11-NTD outward toward the solvent side (Agrawal et al., 2001). This small change in the position of the L11-NTD, in turn, results in movement of the L7/L12-CTD toward the G′ domain of EF-G. Because of well-defined densities for L7/L12-CTD in our maps of EF-G bound ribosome and constraints imposed by the UG mass in defining the position of the G′ domain of EF-G, we are now able to delineate the location and movement of L7/L12-CTD. Previous biochemical studies (Mohr et al., 2002) have shown that EF-G has high affinity for the ribosome in the GTP state but significantly lower affinity in the GDP state; thus, after GTP hydrolysis and P_i release, EF-G is released from the ribosome. In this case, the above-mentioned outward movement of a hook-like feature of the L7/L12-CTD (see Figures 5B and 5C) and interaction of the feature with the tip of the G′ domain of EF-G might assist in the release of EF-G from the ribosome. It is conceivable that the L7/L12-CTD has dynamic and diverse roles in ribosome function, including the recognition and recruitment of various translational factors, the triggering of GTP hydrolysis-related events, and, finally, the removal of those factors from the ribosome.

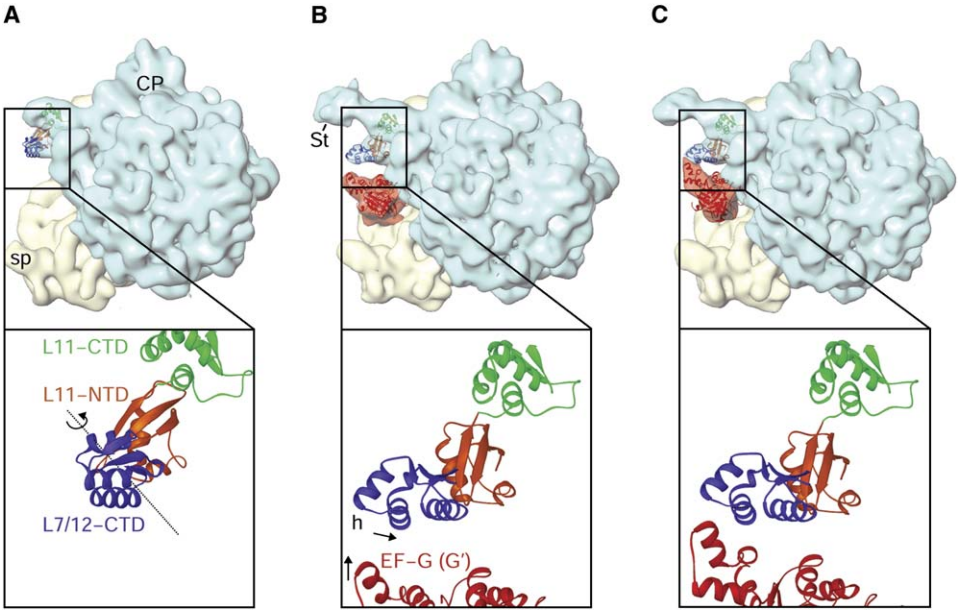

Figure 5. Interactions among the L11-NTD, the L7/L12-CTD, and the G′ Domain of EF-G upon EF-G Binding to the Ribosome and upon GTP Hydrolysis

(A) Control 70S ribosome, (B) 70S•EF-G-209C•GMPPCP complex, and (C) 70S•EF-G-209C•GDP•fusidic acid complex. Atomic structures (ribbons) of the CTD of L7/L12 (blue), L11 (NTD, orange; CTD, green), and a portion of the G domain of EF-G (red) are shown enlarged below. Other landmark includes: h, hook-like feature of the CTD of L7/L12. The axis of rotation of the L7/L12-CTD and the directions of movements of the L7/L12-CTD and G′ domain of EF-G are indicated.

In conclusion, our results trace the movement of a single amino acid that is strategically located on the G′ domain of EF-G during an important step of translocation. As a result of the signal coming from the UG tag on that amino acid, we could delineate the domain boundary as well as the boundary's spatial shift from the shift in position of the UG density peak between the cryo-EM maps representing the two functional states. Definition of the boundaries of EF-G and protein L11 (due to better resolution of structural features) in the ribosome•EF-G maps has allowed us to reconcile several decades of biochemical data and to determine a direct role of the L7/L12-CTD in an EF-G-dependent reaction. We note that further work will be needed to more precisely define the orientation of the L7/L12-CTD within the ALC, through placement of a single UG tag on the L7/L12-CTD. A further achievement of our study is its clear demonstration—as a precedent for the general application of the technique to large, asymmetric, RNA-containing macromolecular assemblies—that the localization of a heavy-metal label in 3D is practicable, despite the fact that in 2D projection, the signal due to the small metal cluster of UG is swamped by the signal due to the RNA.

Experimental Procedures

Preparation of Ribosome and Mutant EF-G

Ribosomes were isolated from *E. coli* strain MRE600 as described earlier (Agrawal and Burma, 1996) by using the buffer system of Blaha and coworkers (Blaha et al., 2000). Also, we applied a very mild salt-wash step with 0.35 M NH_4Cl in place of the 1 M NH_4Cl used by Agrawal and Burma (1996). The *E. coli* wild-type EF-G gene was cloned into the pQE70 (Qiagen) vector that has a 6x-His tag for Ni-NTA agarose-based purification of the expressed protein. There are three naturally occurring Cys residues in *E. coli* EF-G (Ovchinnikov Yu et al., 1982; Zengel et al., 1984). Because these Cys residues are not located at strategic 3D positions, we replaced them with other amino acids by point mutations (Sambrook et al., 1989) such that the biological activity of EF-G is not affected (also see Wilson and Noller, 1998). All of the three naturally occurring Cys residues from the wild-type EF-G were substituted (C114D, C266A,

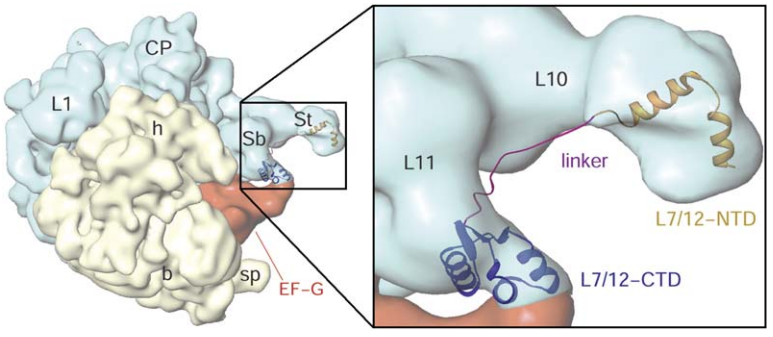

Figure 6. Locations of NTD and CTD of L7/L12 on the Cryo-EM Map of the 70S•EF-G-209C•GDP•Fusidic Acid Complex

The location of the NTD (orange) is derived from a recently published study (Diaconu et al., 2005), whereas the linker polypeptide (magenta) between two domains has been modeled. General locations of protein L10 on the stalk (St) and L11 on the stalk base (Sb) have been marked for reference. All other landmarks are as in previous figures.

and C398S) by using the following primers: 5′-GCGGTAATGGTTTAC GACGCAGTTGGTGGTG-3′, 5′-CGAAATCATCCTGGTAACCGCTG GTTCTGCGTTCAAG-3′, and 5′-GGTGACACCCTGAGTGACCCGGA TGC G-3′, respectively. Subsequently, a Cys residue was introduced at position 209 by substituting the native Ala residue (A209C), with 5′-CGAAGATATCCCGTGTGACATGGTTGAACTGGC-3′ used as the primer. The mutant EF-G gene tagged to 6x-His was overexpressed and initially purified with a Ni-NTA column, followed by final purification on HPLC with a TSK G2000SW (Tosh Biosciences) column.

Preparation of UG/NG-Labeled EF-G-209C

A 10-fold molar excess of monomaleimido-UG or NG (Nanoprobes, Inc., Yaphank, NY) was reacted with the purified EF-G-209C protein. To increase the labeling efficiency, we concentrated the sample by ultrafiltration on a Centricon-3 (Millipore), incubated it for 1 hr at room temperature, and held it overnight at 4ºC for completion of the reaction. The reaction mixture was then subjected to extensive purification on HPLC, using a TSK G2000SW (Tosh Biosciences) column to purify the UG/NG-labeled protein. The peaks showing high absorbance at both 280 nm and 420 nm were pooled as EF-G-209C-UG/NG. For 100% labeling, the ratio of A_{280} to A_{420} would be ~8.2; it was ~7.8 in our experiments, suggesting the presence of ~95% labeled EF-G in the pooled fractions (see Figure S1). It should be noted that the purity of UG-labeled EF-G-209C was most critical in the cryo-EM visualization of the UG mass. The UG/NG-labeled protein was concentrated with Centricon-30, and the buffer was changed to ribosome binding buffer (Agrawal et al., 1998) containing 20 mM HEPES-KOH (pH 7.5), 6 mM $MgCl_2$, 150 mM NH_4Cl, 2 mM spermidine, and 0.4 mM spermine for subsequent reactions. The UG-labeled EF-G was biologically active, as verified in a ribosome-dependent GTPase assay (Nishizuka and Lipmann, 1966).

Preparation of Ribosomal Complexes for Electron Microscopy

Complexes of the 70S ribosome with UG- or NG-labeled or unlabeled EF-G-209C were prepared by using the conditions described previously (Agrawal et al., 1999). The extent of binding of EF-G-209C-UG to the 70S ribosome in all complexes was similar to the binding obtained for unlabeled-EF-G-209C, as assessed by SDS-PAGE. A silver staining kit (Bio-Rad) was used to stain the gel (Figure 1A).

Cryo-Electron Microscopy and Image Processing

Cryo-EM grids were prepared following standard procedures (Wagenknecht et al., 1988). EM data were collected under low-dose conditions on a Philips Tecnai F20 field-emission-gun electron microscope at 200 kV, at a magnification of 50,760×. The cryo-EM data were collected at between 0.7 and 3.5 μm under focus; however, the majority of the data were acquired at close-to-focus settings, between 0.7 and 1.7 μm under focus. The micrographs were digitized with a step size of 14 μm on a Zeiss/Imaging scanner (Z/I Imaging Corporation, Huntsville, AL), corresponding to 2.76 Å on the object scale. The three-dimensional reconstructions were calculated using the 3D projection alignment procedure (Penczek et al., 1994). Each data set was subdivided into defocus groups and then analyzed with SPIDER software (Frank et al., 1996) to obtain CTF-corrected 3D cryo-EM maps (Penczek et al., 1997). Resolutions of maps computed in this study were in the 11.2–12.2 Å range, according to the FSC criterion with a 0.5 cutoff (Bottcher et al., 1997; Malhotra et al., 1998), or in the 7.8–9.0 Å range, according to the considerably more lenient 3σ cutoff criterion (Orlova et al., 1997). However, we used the 0.5 cutoff to filter our maps. The final numbers of images used in each reconstruction and the resolutions of various maps obtained for this study are listed in Table S1. X-ray solution scattering data for the ribosome were used for Fourier amplitude correction (Gabashvili et al., 2000). We also computed 3D maps for all four complexes by exclusively using the subsets of the data that had been collected at close-to-focus settings (between 0.7 and 1.7 μm under focus). The 3D maps obtained in this narrower defocus range should produce more sharply defined peaks for the electron-dense heavy metal clusters (Wagenknecht et al., 1994).

Docking of Atomic Coordinates into the Cryo-EM Maps

To optimally incorporate the X-ray crystallographic structure of the EF-G (AEvarsson et al., 1994; PDB ID code 1ELO), we fitted individual domains of the structure into our cryo-EM maps of ribosome-EF-G complexes in various functional states, by using molecular modelling package O (Jones et al., 1991). The G′ domain within domain I was separately fitted by using a combination of manual rigid-body docking and flexible docking (Wriggers et al., 2000) approaches and by taking into consideration both the cryo-EM envelope and the positional constraints imposed by the UG density. During this process, the distance between residue C209 of EF-G and the position of the UG density was maintained at 16 Å. All resulting coordinates of EF-G were energy-minimized, to relieve strain from any unfavorable steric interactions. We also obtained several independent fittings of the X-ray structure without using any gold-label constraints. However, errors in these fittings were larger than expected, with an up to 3.3 Å shift in the direction of the unconstrained, empty ALC.

In order to obtain an optimum fit of protein L11 in the stalk-base region of the GDP-state map, we introduced only a minor rotation between two conserved proline residues present in the interdomain linker region (Wimberly et al., 1999; PDB code 1MMS) such that the tip of L11-NTD moved by ~2 Å toward the solvent side from its position in the GTP state. However, no changes were made in the X-ray crystallographic structures of L7/L12-CTD (Leijonmarck and Liljas, 1987; PDB code 1CTF) and L7/L12-NTD (Wahl et al., 2000; PDB code 1DD4) to fit them into any of the cryo-EM maps. Docking of the L7/L12-NTD was based on a recent study by Diaconu and coworkers (2005). The CCC values between the fitted X-ray coordinates and the corresponding cryo-EM density maps were determined after conversion of the fitted coordinates into the density map, through computation of averaged densities within volume elements scale matched to those of the cryo-EM map (i.e., with a pixel size of 2.76 Å and after filtration of the X-ray map to the resolution of the cryo-EM density map). The achievable accuracy of fittings of atomic structures into cryo-EM maps has been estimated to be in the range of 1/6 to 1/10 of the resolution of the cryo-EM map (see Rossmann, 2000); this would yield ~1.6 Å in our case.

Visualization of the fitted atomic structures and the cryo-EM density maps was done with Ribbons (Carson, 1991) and IRIS EXPLORER (Numerical Algorithms group, Inc., Downers Grove, IL), respectively. Insight II (Accelrys Inc., USA), with the molecular mechanics/dynamics program DISCOVER, was used to perform energy minimization.

Supplemental Data

Supplemental Data including three figures and one table are available online with this article at http://www.molecule.org/cgi/content/full/20/5/723/DC1/.

Acknowledgments

The authors thank Timothy Booth for help with some of the EM data collections; Melissa Breedlove for help with image processing; and Drs. Chandana Barat and Adriana Verschoor for critically reading the manuscript. This work was supported through the National Institutes of Health (NIH) grant R01 GM61576 to R.K.A. The authors also acknowledge NIH grant R37 GM29169 (to J.F.); the Wadsworth Center's Biochemistry Core facility; and National Science Foundation grant DBI9871347 for EM infrastructure.

Received: August 27, 2005
Revised: September 30, 2005
Accepted: October 25, 2005
Published: December 8, 2005

References

AEvarsson, A., Brazhnikov, E., Garber, M., Zheltonosova, J., Chirgadze, Y., al-Karadaghi, S., Svensson, L.A., and Liljas, A. (1994). Three-dimensional structure of the ribosomal translocase: elongation factor G from *Thermus thermophilus*. EMBO J. *13*, 3669–3677.

Agrawal, R.K., and Burma, D.P. (1996). Sites of ribosomal RNAs involved in the subunit association of tight and loose couple ribosomes. J. Biol. Chem. *271*, 21285–21291.

Agrawal, R.K., Penczek, P., Grassucci, R.A., and Frank, J. (1998). Visualization of elongation factor G on the *Escherichia coli* 70S

ribosome: the mechanism of translocation. Proc. Natl. Acad. Sci. USA *95*, 6134–6138.

Agrawal, R.K., Heagle, A.B., Penczek, P., Grassucci, R.A., and Frank, J. (1999). EF-G-dependent GTP hydrolysis induces translocation accompanied by large conformational changes in the 70S ribosome. Nat. Struct. Biol. *6*, 643–647.

Agrawal, R.K., Linde, J., Sengupta, J., Nierhaus, K.H., and Frank, J. (2001). Localization of L11 protein on the ribosome and elucidation of its involvement in EF-G-dependent translocation. J. Mol. Biol. *311*, 777–787.

Agrawal, R.K., Sharma, M.R., Kiel, M.C., Hirokawa, G., Booth, T.M., Spahn, C.M., Grassucci, R.A., Kaji, A., and Frank, J. (2004). Visualization of ribosome-recycling factor on the *Escherichia coli* 70S ribosome: functional implications. Proc. Natl. Acad. Sci. USA *101*, 8900–8905.

Allen, G.S., Zavialov, A., Gursky, R., Ehrenberg, M., and Frank, J. (2005). The cryo-EM structure of a translation initiation complex from *Escherichia coli*. Cell *121*, 703–712.

Al-Bassam, J., Ozer, R.S., Safer, D., Halpain, S., and Milligan, R.A. (2002). MAP2 and tau bind longitudinally along the outer ridges of microtubule protofilaments. J. Cell Biol. *157*, 1187–1196.

Blaha, G., Stelzl, U., Spahn, C.M., Agrawal, R.K., Frank, J., and Nierhaus, K.H. (2000). Preparation of functional ribosomal complexes and effect of buffer conditions on tRNA positions observed by cryo-electron microscopy. Methods Enzymol. *317*, 292–309.

Bottcher, B., Wynne, S.A., and Crowther, R.A. (1997). Determination of the fold of the core protein of hepatitis B virus by electron cryomicroscopy. Nature *386*, 88–91.

Carson, M. (1991). Ribbons 2.0. J. Appl. Crystallogr. *24*, 103–106.

Czworkowski, J., Wang, J., Steitz, T.A., and Moore, P.B. (1994). The crystal structure of elongation factor G complexed with GDP, at 2.7 Å resolution. EMBO J. *13*, 3661–3668.

Dey, D., Oleinikov, A.V., and Traut, R.R. (1995). The hinge region of *Escherichia coli* ribosomal protein L7/L12 is required for factor binding and GTP hydrolysis. Biochimie *77*, 925–930.

Dey, D., Bochkariov, D.E., Jokhadze, G.G., and Traut, R.R. (1998). Cross-linking of selected residues in the N- and C-terminal domains of *Escherichia coli* protein L7/L12 to other ribosomal proteins and the effect of elongation factor Tu. J. Biol. Chem. *273*, 1670–1676.

Diaconu, M., Kothe, U., Schlunzen, F., Fischer, N., Harms, J.M., Tonevitsky, A.G., Stark, H., Rodnina, M.V., and Wahl, M.C. (2005). Structural basis for the function of the ribosomal L7/L12 stalk in factor binding and GTPase activation. Cell *121*, 991–1004.

Frank, J., and Agrawal, R.K. (2000). A ratchet-like inter-subunit reorganization of the ribosome during translocation. Nature *406*, 318–322.

Frank, J., and Agrawal, R.K. (2001). Ratchet-like movements between the two ribosomal subunits: their implications in elongation factor recognition and tRNA translocation. Cold Spring Harb. Symp. Quant. Biol. *66*, 67–75.

Frank, J., Radermacher, M., Penczek, P., Zhu, J., Li, Y., Ladjadj, M., and Leith, A. (1996). SPIDER and WEB: processing and visualization of images in 3D electron microscopy and related fields. J. Struct. Biol. *116*, 190–199.

Frank, J., Penczek, P., Agrawal, R.K., Grassucci, R.A., and Heagle, A.B. (2000). Three-dimensional cryoelectron microscopy of ribosomes. Methods Enzymol. *317*, 276–291.

Gabashvili, I.S., Agrawal, R.K., Spahn, C.M., Grassucci, R.A., Svergun, D.I., Frank, J., and Penczek, P. (2000). Solution structure of the *E. coli* 70S ribosome at 11.5 Å resolution. Cell *100*, 537–549.

Gao, H., Sengupta, J., Valle, M., Korostelev, A., Eswar, N., Stagg, S.M., Van Roey, P., Agrawal, R.K., Harvey, S.C., Sali, A., et al. (2003). Study of the structural dynamics of the *E. coli* 70S ribosome using real-space refinement. Cell *113*, 789–801.

Hainfeld, J.F. (1987). A small gold-conjugated antibody label: improved resolution for electron microscopy. Science *236*, 450–453.

Ishitsuka, H., Kuriki, Y., and Kaji, A. (1970). Release of transfer ribonucleic acid from ribosomes. A G factor and guanosine triphosphate-dependent reaction. J. Biol. Chem. *245*, 3346–3351.

Jones, T.A., Zou, J.Y., Cowan, S.W., and Kjeldgaard. (1991). Improved methods for building protein models in electron density maps and the location of errors in these models. Acta Crystallogr. A *47 (Pt.2)*, 110–119.

Kikkawa, M., Okada, Y., and Hirokawa, N. (2000). 15 Å resolution model of the monomeric kinesin motor, KIF1A. Cell *100*, 241–252.

Koteliansky, V.E., Domogatsky, S.P., and Gudkov, A.T. (1978). Dimer state of protein L7/L12 and EF-G-dependent reactions of ribosomes. Eur. J. Biochem. *90*, 319–323.

Leijonmarck, M., and Liljas, A. (1987). Structure of the C-terminal domain of the ribosomal protein L7/L12 from *Escherichia coli* at 1.7 Å. J. Mol. Biol. *195*, 555–579.

Makarov, E.M., Oleinikov, A.V., Zecherle, G.N., and Traut, R.R. (1993). Zero-length cross-linking of the C-terminal domain of *Escherichia coli* ribosomal protein L7/L12 to L10 in the ribosome and in the (L7/L12)4–L10 pentameric complex. Biochimie *75*, 963–969.

Malhotra, A., Penczek, P., Agrawal, R.K., Gabashvili, I.S., Grassucci, R.A., Burkhardt, N., Jünemann, R., Nierhaus, K.H., and Frank, J. (1998). *E. coli* 70S ribosome at 15 Å resolution by cryo-electron microscopy: localization of fMet-tRNA$_f^{Met}$ and fitting of L1 protein. J. Mol. Biol. *280*, 103–116.

Mohr, D., Wintermeyer, W., and Rodnina, M.V. (2002). GTPase activation of elongation factors Tu and G on the ribosome. Biochemistry *41*, 12520–12528.

Montesano-Roditis, L., Glitz, D.G., Traut, R.R., and Stewart, P.L. (2001). Cryo-electron microscopic localization of protein L7/L12 within the *Escherichia coli* 70 S ribosome by difference mapping and Nanogold labeling. J. Biol. Chem. *276*, 14117–14123.

Nishizuka, Y., and Lipmann, F. (1966). Comparison of guanosine triphosphate split and polypeptide synthesis with a purified *E. coli* system. Proc. Natl. Acad. Sci. USA *55*, 212–219.

Orlova, E.V., Dube, P., Harris, J.R., Beckman, E., Zemlin, F., Markl, J., and van Heel, M. (1997). Structure of keyhole limpet hemocyanin type 1 (KLH1) at 15 Å resolution by electron cryomicroscopy and angular reconstitution. J. Mol. Biol. *271*, 417–437.

Ovchinnikov Yu, A., Alakhov Yu, B., Bundulis Yu, P., Bundule, M.A., Dovgas, N.V., Kozlov, V.P., Motuz, L.P., and Vinokurov, L.M. (1982). The primary structure of elongation factor G from *Escherichia coli*. A complete amino acid sequence. FEBS Lett. *139*, 130–135.

Pape, T., Wintermeyer, W., and Rodnina, M.V. (1998). Complete kinetic mechanism of elongation factor Tu-dependent binding of aminoacyl-tRNA to the A site of the *E. coli* ribosome. EMBO J. *17*, 7490–7497.

Parmeggiani, A., and Sander, G. (1981). Properties and regulation of the GTPase activities of elongation factors Tu and G, and of initiation factor 2. Mol. Cell. Biochem. *35*, 129–158.

Penczek, P.A., Grassucci, R.A., and Frank, J. (1994). The ribosome at improved resolution: new techniques for merging and orientation refinement in 3D cryo-electron microscopy of biological particles. Ultramicroscopy *53*, 251–270.

Penczek, P.A., Zhu, J., Schroder, R., and Frank, J. (1997). Three-dimensional reconstruction with contrast transfer function compensation from defocus series. Scanning Microsc. *11*, 147–154.

Rodnina, M.V., Pape, T., Fricke, R., Kuhn, L., and Wintermeyer, W. (1996). Initial binding of the elongation factor Tu.GTP.aminoacyl-tRNA complex preceding codon recognition on the ribosome. J. Biol. Chem. *271*, 646–652.

Rodnina, M.V., Savelsbergh, A., Katunin, V.I., and Wintermeyer, W. (1997). Hydrolysis of GTP by elongation factor G drives tRNA movement on the ribosome. Nature *385*, 37–41.

Rossmann, M.G. (2000). Fitting atomic models into electron-microscopy maps. Acta Crystallogr. D Biol. Crystallogr. *56*, 1341–1349.

Safer, D. (1999). Undecagold cluster labeling of proteins at reactive cysteine residues. J. Struct. Biol. *127*, 101–105.

Safer, D., Bolinger, L., and Leigh, J.S., Jr. (1986). Undecagold clusters for site-specific labeling of biological macromolecules: simplified preparation and model applications. J. Inorg. Biochem. *26*, 77–91.

Sambrook, J., Fritsch, E.F., and Maniatis, T. (1989). Molecular Cloning: A Laboratory Manual, Second Edition (Cold Spring Harbor, NY: Cold Spring Harbor Laboratory Press).

Savelsbergh, A., Mohr, D., Wilden, B., Wintermeyer, W., and Rodnina, M.V. (2000). Stimulation of the GTPase activity of translation elongation factor G by ribosomal protein L7/L12. J. Biol. Chem. *275*, 890–894.

Sharma, M.R., Barat, C., Wilson, D.N., Booth, T.M., Kawazoe, M., Hori-Takemoto, C., Shirouzu, M., Yokoyama, S., Fucini, P., and Agrawal, R.K. (2005). Interaction of Era with the 30S ribosomal subunit: implications for 30S subunit assembly. Mol. Cell *18*, 319–329.

Sommer, A., Etchison, J.R., Gavino, G., Zecherle, N., Casiano, C., and Traut, R.R. (1985). Preparation and characterization of two monoclonal antibodies against different epitopes in *Escherichia coli* ribosomal protein L7/L12. J. Biol. Chem. *260*, 6522–6527.

Stark, H., Rodnina, M.V., Rinke-Appel, J., Brimacombe, R., Wintermeyer, W., and van Heel, M. (1997). Visualization of elongation factor Tu on the *Escherichia coli* ribosome. Nature *389*, 403–406.

Stark, H., Rodnina, M.V., Wieden, H.J., van Heel, M., and Wintermeyer, W. (2000). Large-scale movement of elongation factor G and extensive conformational change of the ribosome during translocation. Cell *100*, 301–309.

Traut, R.R., Dey, D., Bochkariov, D.E., Oleinikov, A.V., Jokhadze, G.G., Hamman, B., and Jameson, D. (1995). Location and domain structure of *Escherichia coli* ribosomal protein L7/L12: site specific cysteine crosslinking and attachment of fluorescent probes. Biochem. Cell Biol. *73*, 949–958.

Valle, M., Zavialov, A., Sengupta, J., Rawat, U., Ehrenberg, M., and Frank, J. (2003). Locking and unlocking of ribosomal motions. Cell *114*, 123–134.

van Agthoven, A.J., Maassen, J.A., Schrier, P.I., and Moller, W. (1975). Inhibition of EF-G dependent GTPase by an aminoterminal fragment of L7/L12. Biochem. Biophys. Res. Commun. *64*, 1184–1191.

Wagenknecht, T., Grassucci, R., and Frank, J. (1988). Electron microscopy and computer image averaging of ice-embedded large ribosomal subunits from *Escherichia coli*. J. Mol. Biol. *199*, 137–147.

Wagenknecht, T., Berkowitz, J., Grassucci, R., Timerman, A.P., and Fleischer, S. (1994). Localization of calmodulin binding sites on the ryanodine receptor from skeletal muscle by electron microscopy. Biophys. J. *67*, 2286–2295.

Wahl, M.C., Bourenkov, G.P., Bartunik, H.D., and Huber, R. (2000). Flexibility, conformational diversity and two dimerization modes in complexes of ribosomal protein L12. EMBO J. *19*, 174–186.

Wilson, K.S., and Noller, H.F. (1998). Mapping the position of translational elongation factor EF-G in the ribosome by directed hydroxyl radical probing. Cell *92*, 131–139.

Wimberly, B.T., Guymon, R., McCutcheon, J.P., White, S.W., and Ramakrishnan, V. (1999). A detailed view of a ribosomal active site: the structure of the L11-RNA complex. Cell *97*, 491–502.

Wittmann-Liebold, B. (1985). Ribosomal proteins: their structure and evolution. In Structure, Function and Genetics of Ribosomes, B. Hardesty and G. Kramer, eds. (New York, NY: Springer), pp. 326–361.

Wriggers, W., Agrawal, R.K., Drew, D.L., McCammon, A., and Frank, J. (2000). Domain motions of EF-G bound to the 70S ribosome: insights from a hand-shaking between multi-resolution structures. Biophys. J. *79*, 1670–1678.

Zecherle, G.N., Oleinikov, A., and Traut, R.R. (1992). The C-terminal domain of *Escherichia coli* ribosomal protein L7/L12 can occupy a location near the factor-binding domain of the 50S subunit as shown by cross-linking with N-[4-(p-azidosalicylamido)butyl]-3-(2′-pyridyldithio)propionamide. Biochemistry *31*, 9526–9532.

Zengel, J.M., Archer, R.H., and Lindahl, L. (1984). The nucleotide sequence of the *Escherichia coli* fus gene, coding for elongation factor G. Nucleic Acids Res. *12*, 2181–2192.

Accession Numbers

Relevant coordinates of the fitted X-ray crystallographic structures of ribosomal proteins L11 and L7/L12 and EF-G into the cryo-EM map of the 70S•EF-G-209C•GDP•fusidic acid complex have been deposited in the Protein Data Bank, http://www.rcsb.org/pdb/ (PDB ID code 2BCW).